JOC The Journal of Organic Chemistry

Article

pubs.acs.org/joc

An Evolving Insight into Chiral H-Bond Catalyzed Aza-Henry Reactions: A Cooperative Role for Noncovalent Attractive Interactions Unveiled by Density Functional Theory

Seyedeh Maryamdokht Taimoory and Travis Dudding*

Brock University, 1812 Sir Isaac Brock Way, St. Catharines, ON, L2S 3A1 Canada

Supporting Information

ABSTRACT: The role of cooperative effects arising from noncovalent attractive interactions as a vital factor governing stereoinduction in chiral H-bond catalyzed aza-Henry reactions is reported. Supporting this finding were density functional theory (DFT) calculations which revealed a shape and size dependency existed between the catalyst and substrates that when matched lead to high enantioselectivity, as reflected by favorable activation parameters. Associated with optimal catalyst and substrate pairing were a closed catalytic binding pocket and a synclinal orientation of the substrates that reinforced favorable stereoelectronic effects and dispersive type forces. Meanwhile, unfavorable steric interactions were found to be a dominant effect controlling diastereoselection.

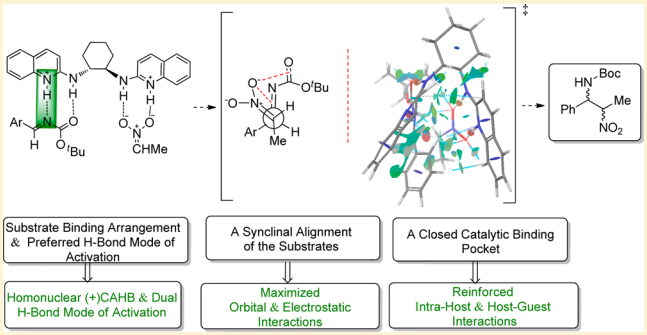

INTRODUCTION

Hydrogen bonding (H-bonding)[1] bridges nearly all of life's underlying chemical processes for which enzymes with near-mastery have evolved to harness this binding force to great effect. Nowhere is this truer than in terms of catalysis. Lacking such evolutionary prowess, chemists in strategic recourse have in recent decades, especially since the rise of organocatalysts, embarked upon the advancement of H-bond catalysts that in many ways rival enzymes.[2] Attesting to this fact have been a number of chiral guanidine,[3] cinchona alkaloid,[4] peptide,[5] and (thio)urea[6] organocatalysts that employ bifunctional and/or multifunctional H-bonding manifolds to orchestrate catalysis with high proficiency and stereocontrol by what are thought provoking mechanisms of action that reserve elements of enzymatic biomimicry. While these parallels pose several intriguing questions in terms of rate acceleration and stereoselectivity that if well-understood would offer potential innovative insight for designing future generations of chiral H-bond organocatalysts, there remains much to be learned in this regard. Overshadowing and arguably complicating this prospect, however, has been the H-bond itself as it continues to be a debated topic based upon its electrostatic "dipole–dipole" vs "partial covalent" character.[7]

Prevalent throughout Nature as well are attractive noncovalent interactions,[8] such as H-bonding, $\pi\cdots\pi$, anion$\cdots\pi$, cation$\cdots\pi$, and X–H$\cdots\pi$ interactions which embody another binding force governing reactivity and selectivity. Meanwhile the synergistic versus antagonistic[9] interplay of noncovalent interactions arising from H-bonding and/or other noncovalent interactions referred to as "cooperativity effects" presents a great uncertainty in the context of catalytic mechanistic rationale,[10] despite being heavily studied and more conceptually well-established in many other fields of science ranging from biology, materials science, molecular recognition, and supramolecular chemistry, among others.[11]

Given the above limitations, amidiniums[12] typify a decidedly interesting state-of-the-art class of organocatalyst owing to the potential to form polarized (positively charged) H-bonds, ability to delocalize positive charge over several atoms, and lack of mechanistic study, which is particularly true in terms of computational based mechanistic rationale. In this regard, Johnston and co-workers'[13] advancement of a class of a chiral Brønsted acidic amidinium based H-bond catalysts [e.g., HQuin-BAM (**1**)] have been shown to catalyze a number of asymmetric transformations, perhaps most notably being aza-Henry reactions with high selectivity and good product yields (Scheme 1). Unique to this amidinium organocatalyst framework, however, relative to most contemporary H-bond catalysts is its mode of action. More to the point, unlike the mainstream of H-bond catalysts, which facilitates catalysis through bifunctional, cooperative, and resonance enhanced H-bonding, it was suggested early on that HQuin-BAM and congeners utilized polar ionic H-bonding to catalyze reactions.[13a] A more recent computational study by our group[14] established that the modus operandi of HQuin-BAM catalysis in aza-Henry reactions involved positive charge assisted H-bonding, that is, a (+)CAHB manifold.[15] Manifesting from this preliminary work as well were the telling signs of cooperativity effects stemming from H-bonding and other classes of noncovalent interactions

Received: February 3, 2016
Published: March 23, 2016

DOI: 10.1021/acs.joc.6b00248
J. Org. Chem. 2016, 81, 3286–3295

Scheme 1. HQuin-BAM Catalyzed Asymmetric Aza-Henry Reactions

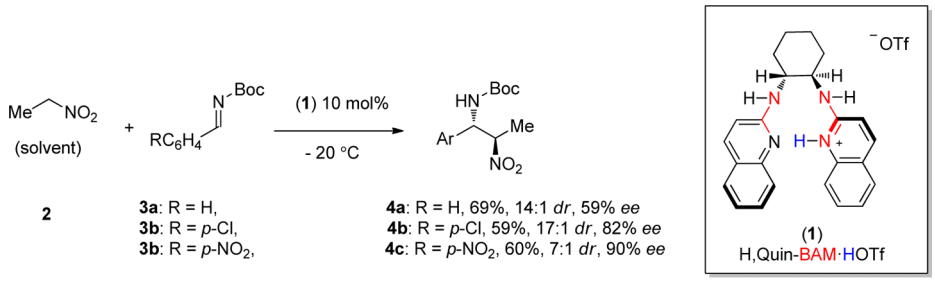

that at the time were not extensively investigated, as it was deemed more vital to establish basic insight into the preferred modes of H-bonding and their effect on enantioselection in aza-Henry reactions. Intrigued by these early indications of cooperativity effects having a role in these aza-Henry reactions, we recently initiated studies to elucidate if this is indeed the case. Emerging from these studies and as detailed herein is the finding that cooperativity effects arising from H-bonding and other intramolecular (intrahost) and intermolecular (host−guest) noncovalent interactions between the catalyst (host molecule) and substrates (guest molecules) serve a critical role in HQuin-BAM catalyzed aza-Henry reactions, especially in terms of rate acceleration and more effective catalyst−substrate binding associated with enthalpic advantages and small entropic penalties, as well as stereoselection.

COMPUTATIONAL DETAILS

All calculations were performed with the Gaussian 09[16] suite of programs at the density functional theory (DFT) level employing both Grimme's dispersion corrected functional B3LYP-D3[17] and dual-corrected ωB97X-D functional,[18] within the IEF-PCM model[19] to gain a more accurate treatment of medium/long ranged attractive noncovalent interactions (default solvent parameters for nitroethane were applied). All of the optimized geometries were confirmed by frequency computations as minima (zero imaginary frequencies) or transition structures (one imaginary frequency). Single-point calculations were also performed at B3LYP/6-31G(d), ωB97X-D/6-311+G(d,p), and B3LYP-D3/6-311+G(d,p) levels on ωB97X-D/6-31G(d) optimized geometries. Thermal corrections from the vibrational frequencies at the ωB97X-D/6-31G(d) were added to the electronic energies of the abovementioned methods to gain the free energies.[20] Natural bond orbital analysis and natural population analysis (NPA) were performed with NBO version 3.1 implemented in Gaussian 09.[21] A topological analysis of the electron density was carried out with Bader's quantum theory of atoms in molecules (QTAIM) using the AIM2000 software.[22] The noncovalent interactions (NCI) index analysis was performed using the Schrödinger Jaguar program, and the results were visualized with Maestro 10.1.[23] Further distortion/interaction analysis[24] was used to inspect the origin of the energy difference between the stereo-determining transition states. Based on the distortion/interaction analysis, the activation barrier, $\Delta E^{\ddagger}$, is subdivided into (1) the interaction energy between the distorted catalyst and the two substrates in their transition state geometry, ΔE_{int}; (2) the destabilizing distortion of the catalyst at the transition state geometry compared with its ground state, $\Delta E_{dist(cat)}$; and (3) the distortion/interaction energy between the two reacting substrates at the transition state relative to their ground states, $\Delta E_{dist(subs)}$.

RESULTS AND DISCUSSION

Having recently reported a preliminary study addressing the mechanism and origin of enantioselectivity in HQuin-BAM catalyzed aza-Henry reactions,[14] we were drawn toward the prospect of carrying out a more compressive study providing insight into the source(s) of enantio- and diastereoselection in these catalytic processes. To this end, it was reasoned that having a firm grasp of the factors allowing HQuin-BAM to impart high enantio- and diastereoselectivity to aza-Henry reactions would provide valuable mechanistic insight for designing future catalysts having better performance characteristics. Accordingly, the experimental finding[13a] that HQuin-BAM catalyzed the addition of nitroethane **2** to *N*-Boc phenylaldimine **3a** with high 14:1 *anti*/*syn* dr to afford (1*R*,2*S*)-configured product **4a** in 59% ee was taken as a point of departure for this study due to its minimalist structural nature, while still being a diastereoselective example (Scheme 1).

Thus, an initial series of transition state searches were performed in which the relative N−C−C−N dihedral angle (θ_{NCCN}) around the developing C−C bond and (*Re*)- vs (*Si*)-stereofacial mode of nitronate (generated *in situ* from nitroethane) addition to *N*-Boc aldimine, as well as the orientation of the *N*-Boc aldimine (flipped by 180°) with respect to the HQuin-BAM catalyst, were varied. Taken into consideration also was the binding of only the aldimine and/or nitronate by the HQuin-BAM catalyst. Emerging from these searches were three structurally different low energy (*Re*)- and (*Si*)-selective addition modes involving (1) a bidentate H-bond activated aldimine and unbound nitronate, mode A ($\mathbf{TS1}_{A(h)}$ and $\mathbf{TS1}_{A(het)}$); (2) an unbound aldimine and a bicoordinated H-bond stabilized nitronate, mode B ($\mathbf{TS1}_{B(h)}$ and $\mathbf{TS1}_{B(het)}$); and (3) dual H-bond stabilization of nitronate and aldimine activation, mode C ($\mathbf{TS1}_{C(h)}$ and $\mathbf{TS1}_{C(het)}$) (see Supporting Information for the energy and structure of each addition mode). Further two potential binding orientations between the aldimine and the catalyst involving either homonuclear (N^+−H···N) or heteronuclear (N^+−H···O) positive charged assisted hydrogen bonds (+)CAHBs were found in each of these addition modes that were crucial for directing the substrates along optimal attack geometries, stabilizing charge buildup, and enabling transmission of catalyst based chirality to the substrates. Ultimately, this survey produced 24 transition state structures involving homo-/heteronuclear H-bonding leading to *anti*- or *syn*-products with the (1*R*,2*S*), (1*R*,2*R*), (1*S*,2*R*), or (1*S*,2*S*)-configuration, which were labeled as *anti*-(1*R*,2*S*)-$\mathbf{TS}_{A(h)}$, *syn*-(1*R*,2*R*)-$\mathbf{TS}_{B(het)}$, *anti*-(1*S*,2*R*)-$\mathbf{TS}_{C(het)}$, etc.; (h) and (het) designate homo-/heteronuclear H-bonding, A−C refer to the addition mode, and the terms *anti*-(1*R*,2*S*) and *syn*-(1*R*,2*R*) for example indicate the relative configuration and absolute stereochemistry of the product that would be formed.[25] Among the optimized transition states the most favorable was that of addition mode $\mathbf{TS1}_{C(h)}$, wherein the H-bond activated *N*-Boc aldimine was oriented in a manner that maximized the strength of the homonuclear (+)CAHB contact. Within this subset of

DOI: 10.1021/acs.joc.6b00248
J. Org. Chem. 2016, 81, 3286−3295

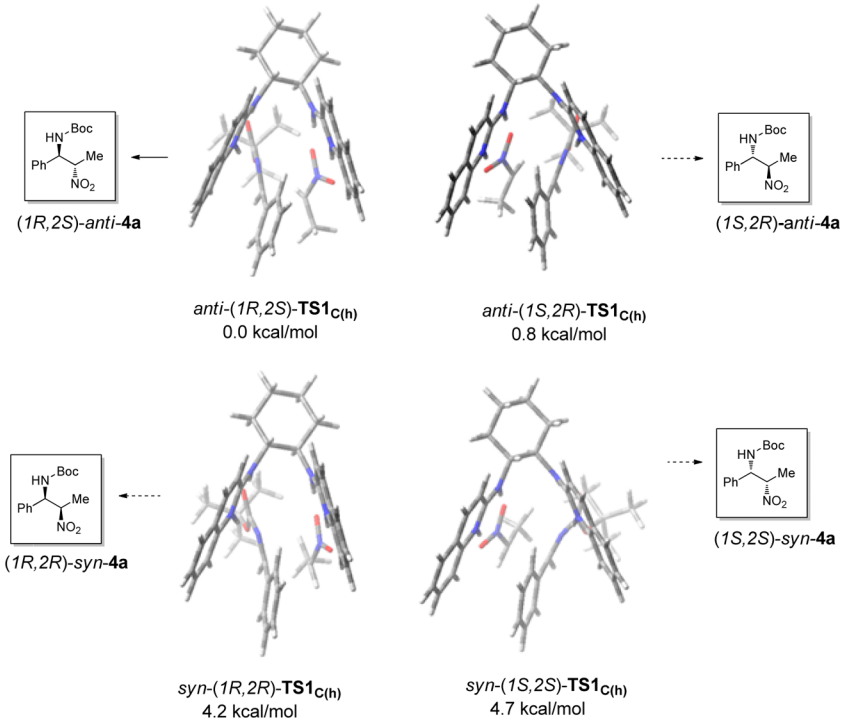

Figure 1. ωB97X-D/6-31G(d) calculated C−C bond forming enantiomeric and diastereomeric transition states, $\mathbf{TS1}_{\mathbf{C(h)}}$.

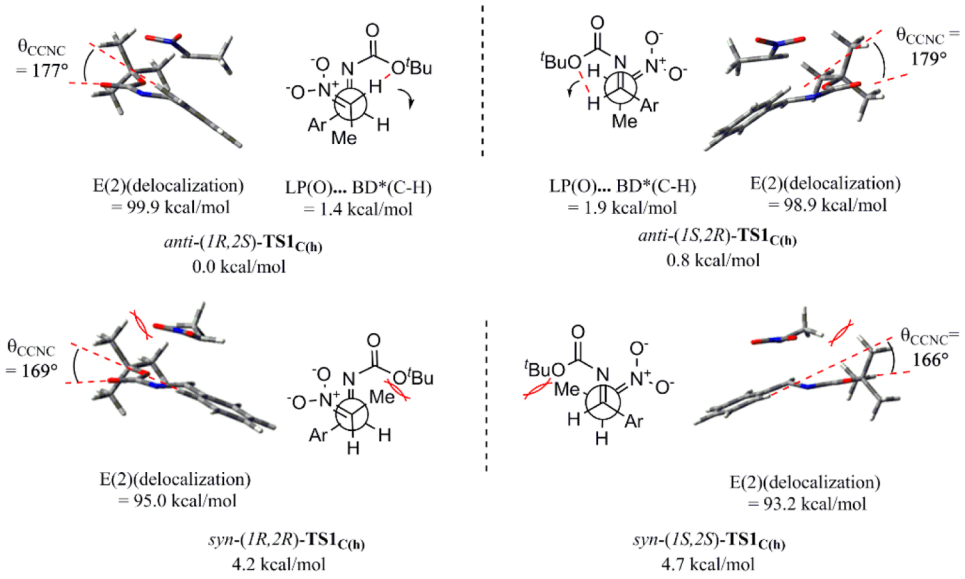

Figure 2. Evaluated resonance stabilization energy and C−C−N−C dihedral angle of the *N*-Boc aldimine in the ωB97X-D/6-31G(d) calculated stereodetermining C−C bond forming transition states $\mathbf{TS1}_{\mathbf{C(h)}}$.

stereomeric structures the two most favorable were *anti*-(1*R*,2*S*)-$\mathbf{TS1}_{\mathbf{C(h)}}$ and *anti*-(1*S*,2*R*)-$\mathbf{TS1}_{\mathbf{C(h)}}$ with relative free energies of 0.0 and 0.8 kcal/mol, whereas the two *syn*-diastereomeric transition states corresponding to *syn*-(1*R*,2*R*)-$\mathbf{TS1}_{\mathbf{C(h)}}$ and *syn*-(1*S*,2*S*)-$\mathbf{TS1}_{\mathbf{C(h)}}$ were 4.2 and 4.7 kcal/mol higher in energy than *anti*-(1*R*,2*S*)-$\mathbf{TS1}_{\mathbf{C(h)}}$ (Figure 1).

As for the basis of this energetic difference a breakdown of the factors contributing to diastereo- vis-à-vis enantioinduction was undertaken to disentangle these two aspects. On this front, the origin of *anti*/*syn*-diastereocontrol was addressed first. Arising from this endeavor was the finding that a decisive factor controlling diastereoinduction was the presence of a sterically unfavorable interaction between the nitronate methyl and the aldimine *N*-Boc protecting group in the higher energy transition states. More specifically, in *syn*-(1*R*,2*R*)-$\mathbf{TS1}_{\mathbf{C(h)}}$ and *syn*-(1*S*,2*S*)-$\mathbf{TS1}_{\mathbf{C(h)}}$ this sterically unfavorable interaction distorted the aldimine from planarity which in turn reduced conjugation in the aldimine π-system as seen by the C−C−N−C dihedral angle of 169° and 166°, whereas the comparable θ_{CCNC} metrics were 177° and 179° in *anti*-(1*R*,2*S*)-$\mathbf{TS1}_{\mathbf{C(h)}}$ and *anti*-(1*S*,2*R*)-$\mathbf{TS1}_{\mathbf{C(h)}}$, Figure 2. Supporting this marginal loss of conjugation in *syn*-(1*R*,2*R*)-$\mathbf{TS1}_{\mathbf{C(h)}}$ and *syn*-(1*S*,2*S*)-$\mathbf{TS1}_{\mathbf{C(h)}}$ was the NBO resonance stabilization energies for electron delocalization in the aldimine π-system that *circa* amounted to 93−95 kcal/mol, while in *anti*-(1*R*,2*S*)-$\mathbf{TS1}_{\mathbf{C(h)}}$ and *anti*-(1*S*,2*R*)-$\mathbf{TS1}_{\mathbf{C(h)}}$ they summed to 99 kcal/mol. Meanwhile, a

DOI: 10.1021/acs.joc.6b00248
J. Org. Chem. 2016, 81, 3286−3295

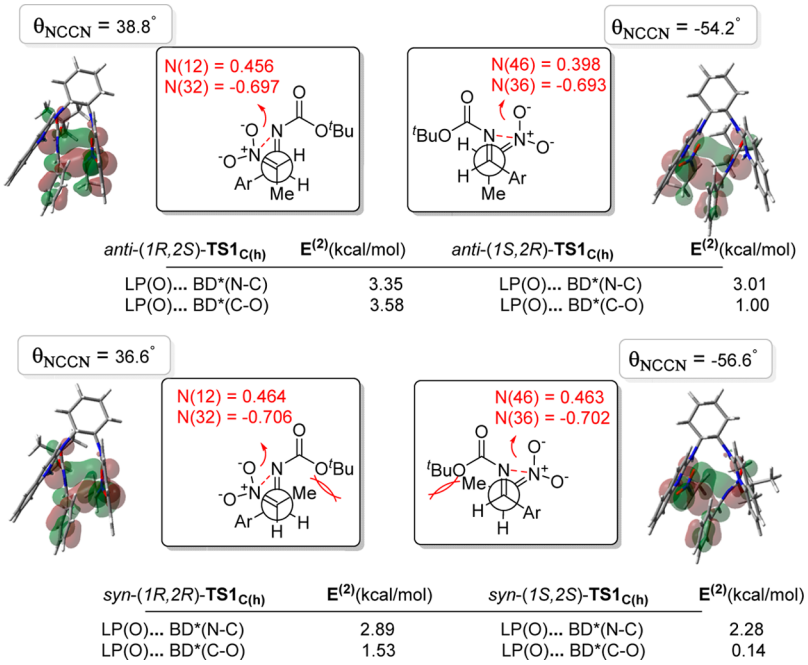

Figure 3. Depiction of the substrate alignment and secondary orbital interactions in the ωB97X-D/6-31G(d) calculated stereodetermining C−C bond forming transition states $\mathbf{TS1}_{C(h)}$. 3D models represent the HOMO orbitals.

small albeit noteworthy "non-classical" H-bonding (NCHB)[26] interaction involving alkoxy oxygen lone pair donation into an antibonding vinylic nitronate C−H σ*-orbital in *anti*-(1*R*,2*S*)-$\mathbf{TS1}_{C(h)}$ and *anti*-(1*S*,2*R*)-$\mathbf{TS1}_{C(h)}$ (E_{NBO} = 1.4 and 1.9 kcal/mol) that was not present in *syn*-(1*R*,2*R*)-$\mathbf{TS1}_{C(h)}$ and *syn*-(1*S*,2*S*)-$\mathbf{TS1}_{C(h)}$ was also found to contribute to *anti*-diastereoselectivity, Figure 2.

Apart from the aforementioned stabilizing C−H···O and destabilizing steric interactions, only marginal structural and stereoelectronic differences existed between these transition states, thus underscoring the significance of these interactions as a crucial factor governing diastereoselectivity given the consistence between the predicted and reported trends.

Origins of (*Si*)/(*Re*) Enantiocontrol. Having pinpointed the principal sources of diastereoselection, our attention turned to identifying the variables responsible for enantioinduction in the preferred (*Si*)-selective transition states, *anti*-(1*R*,2*S*) and *syn*-(1*R*,2*R*)-$\mathbf{TS1}_{C(h)}$, over the (*Re*)-selective first-order saddle points, *anti*-(1*S*,2*R*) and *syn*-(1*S*,2*S*)-$\mathbf{TS1}_{C(h)}$. Emerging from this consideration was the finding of two key factors, namely substrate and catalyst based stereocontrol in conjunction with cooperative effects.

A. Substrate Control of Enantioselection. Relating to the basis of substrate interactions governing enantioselection an assessment of the orbital and electrostatic interactions proved most instructive. More to the point, associated with the similar C−C bond forming distances of 2.23−2.24 Å in *anti*-(1*R*,2*S*)-$\mathbf{TS1}_{C(h)}$, *syn*-(1*R*,2*R*)-$\mathbf{TS1}_{C(h)}$, *anti*-(1*S*,2*R*)-$\mathbf{TS1}_{C(h)}$, and *syn*-(1*S*,2*S*)-$\mathbf{TS1}_{C(h)}$ were a number of stabilizing electrostatic and donor−acceptor orbital interactions between the *N*-Boc aldimine and nitronate substrates that governed (*Si*)- vs (*Re*)-enantiofacial selectivity. For instance, the synclinal attack orientation (θ_{NCCN} = 36.0°−38.0°) found in the (*Si*)-enantioselective transition states resulted in more favorable nitronate oxygen lone pairs donation into antibonding orbitals of the C═O and N═C bonds of the *N*-Boc aldimine, as revealed by the NBO secondary orbital interaction energies, which when summed together lead to total values of 6.93, 4.42, 4.01, and 2.42 kcal/mol for *anti*-(1*R*,2*S*)-$\mathbf{TS1}_{C(h)}$, *syn*-(1*R*,2*R*)-$\mathbf{TS1}_{C(h)}$, *anti*-(1*S*,2*R*)-$\mathbf{TS1}_{C(h)}$, and *syn*-(1*S*,2*S*)-$\mathbf{TS1}_{C(h)}$, respectively (Figure 3). Charge separation also appeared to have a possible role in enantioselection based on the partial positive nitronate N(12) and partial negative aldimine N(32) natural charge assignments (NPA charges) of 0.456 and −0.697 in *anti*-(1*R*,2*S*)-$\mathbf{TS1}_{C(h)}$ and 0.464 and −0.706 in *syn*-(1*R*,2*R*)-$\mathbf{TS1}_{C(h)}$ combined with the comparable $N^{\delta+}\cdots N^{\delta-}$ distances of 2.91 and 2.89 Å in the two structures. Conversely, this interaction was much weaker in the (*Re*)-enantioselective transition states as seen by less positive and negative N(46) and N(36) nitrogen atom charges in *anti*-(1*S*,2*R*)-$\mathbf{TS1}_{C(h)}$ (NPA charges = 0.398, −0.693) and *syn*-(1*S*,2*S*)-$\mathbf{TS1}_{C(h)}$ (NPA charges = 0.463, −0.702), which in comparison possessed greater $N^{\delta+}\cdots N^{\delta-}$ distances of 3.00 and 3.03 Å (Figure 3).

B. Catalyst Control of Enantioselection. Another factor contributing to (*Si*)- vs (*Re*)-enantiofacial selectivity arises from the HQuin-BAM catalyst adopting two different conformations (closed/open) that reinforced/weakened stabilizing intra- (intrahost) and intermolecular (host−guest) noncovalent attractive interactions. Consistent with this conclusion were the relative distances between the two quinolinium rings of the catalyst, as judged from the shorter $C_{(ring\ 1)}-C_{(ring\ 2)}$ and $C_{(ring\ 3)}-C_{(ring\ 4)}$ metrics (C = ring centroid) of 4.50 and 6.50 Å in *anti*-(1*R*,2*S*)-$\mathbf{TS1}_{C(h)}$ and *syn*-(1*R*,2*R*)-$\mathbf{TS1}_{C(h)}$ compared with the alternative distance of 5.00 and 7.50 Å in *anti*-(1*S*,2*R*)-$\mathbf{TS1}_{C(h)}$ and *syn*-(1*S*,2*S*)-$\mathbf{TS1}_{C(h)}$, Figure 4. Associated with the more closed binding pocket of the catalyst in the favored (*Si*)-enantioselective transition states was a smaller intrinsic distortion of the catalyst from the respective ground state geometry as deemed from the computed distortion energies, $E_{dist(cat)}$, of 5.20 and 5.17 kcal/mol for *anti*-(1*R*,2*S*)-$\mathbf{TS1}_{C(h)}$ and *syn*-(1*R*,2*R*)-$\mathbf{TS1}_{C(h)}$, while those of the (*Re*)-enantioselective transition states, *anti*-(1*S*,2*R*)-$\mathbf{TS1}_{C(h)}$ and *syn*-(1*S*,2*S*)-$\mathbf{TS1}_{C(h)}$, were 5.86 and 5.49 kcal/mol (Figure 4; see Supporting Information Table S2). Meanwhile the relative computed

DOI: 10.1021/acs.joc.6b00248
J. Org. Chem. 2016, 81, 3286−3295

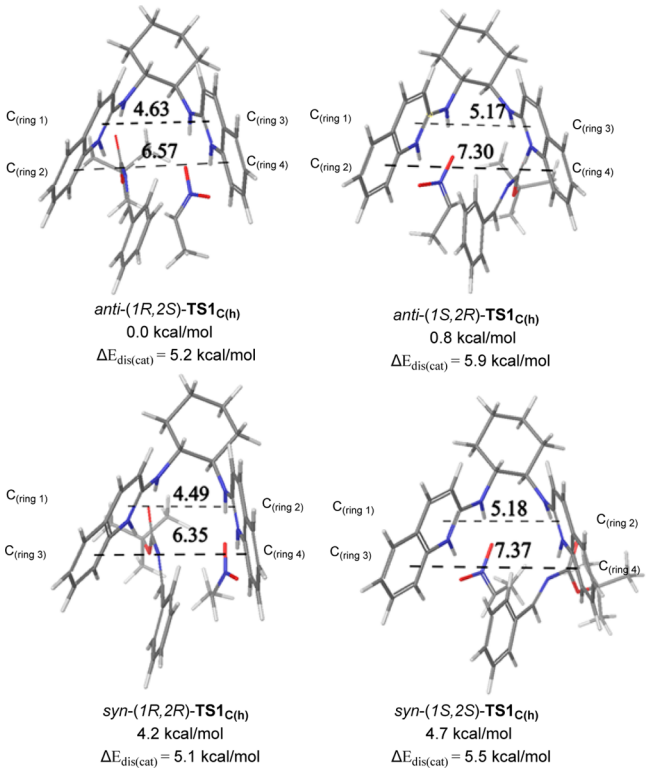

Figure 4. Closed/open catalyst conformations computed at the ωB97X-D/6-31G(d) level for the stereodetermining C−C bond forming transition states $\mathbf{TS1}_{\mathbf{C(h)}}$.

energies of these four transition states differed substantially when using the dispersion-uncorrected functional B3LYP versus the dual-corrected ωB97X-D functional, which considers both dispersion and range separation corrections, and the dispersion-corrected B3LYP-D3 functional (see Supporting Information Table S1).[27] Notably, the predicted trends from the dispersion-corrected functionals were more in line with the reported selectivities, thus, alluding to the potential role of noncovalent attractive interactions originating from dispersion forces (instantaneous multipoles-induced multipoles), electrostatics (dipole−dipole, dipole−quadrupole, etc.), and polarization forces (permanent multipoles-induced multipoles)[28] as being a key factor in stabilizing the stereodetermining transition states.

Intrigued by this finding to better understand the intra- and intermolecular attractive interactions contributing to this energetic difference, noncovalent interaction (NCI) calculations[29] were performed to identify the presence of weakly/moderately attractive (green isosurfaces), repulsive (deep blue isosurfaces) contacts as well as medium strength H-bonding and the developing C−C bond (red features) in these transition states, thus providing from isosurface plots a qualitative visual interpretation. Notably, these calculations also afford NCI interaction critical points (ρ_{ICP}),[29] which allow for quantification of the relative magnitude and significance of noncovalent interactions. Arrived at from these NCI isosurfaces of the (*Si*)-enantioselective transition states was the illuminating presence of several stabilizing intramolecular (intrahost) and intermolecular (host−guest) noncovalent interactions, whereas the favorable NCI isosurface area density was less in the (*Re*)-enantioselective transition states. For clarity the NCI isosurfaces of greatest interest were highlighted in Figure 5. With respect to the intramolecular (intrahost) interactions a weak $\pi_{Ar}\cdots\pi_{Ar}$ type (highlighted as A in Figure 5) between the quinolinium rings in *anti*-(1*R*,2*S*)-$\mathbf{TS1}_{\mathbf{C(h)}}$ and *syn*-(1*R*,2*R*)-$\mathbf{TS1}_{\mathbf{C(h)}}$ were present based on the NCI isosurface plot ρ_{ICP} critical points with values of −0.0037 and −0.0039, thus suggesting the existence of dispersive type interactions. Meanwhile an analogous set of interactions were not present in *anti*-(1*S*,2*R*)-$\mathbf{TS1}_{\mathbf{C(h)}}$ and *syn*-(1*S*,2*S*)-$\mathbf{TS1}_{\mathbf{C(h)}}$. Apparent in both (*Si*)- and (*Re*)-enantioselective transition states as well were two isolated NCI isosurface regions originating from intramolecular (intrahost) interactions between the quinolinium rings and the chiral 1,2-diaminocyclohexane backbone of the catalyst (highlighted as B in Figure 5). This interaction, however, was stronger in the energetically favored (*Si*)-enantioselective transition states (ρ_{ICP} = −0.0111 to −0.0114) compared to the (*Re*)-enantioselective transition states (ρ_{ICP} = −0.0104 to −0.0107). An array of stabilizing intermolecular (host−guest) $N^+-H\cdots\pi_{Ar}$ (highlighted as C in Figure 5) and $\pi_{Ar}\cdots\pi_{Ar}$ or $C-H_{Ar}\cdots\pi_{Ar}$ (highlighted as D in Figure 5) stacking type interactions between the *N*-Boc aldimine and the catalyst quinolinium rings were also present in all of the transition states, though these contacts were stronger and broader in *anti*-(1*R*,2*S*)-$\mathbf{TS1}_{\mathbf{C(h)}}$ and *syn*-(1*R*,2*R*)-$\mathbf{TS1}_{\mathbf{C(h)}}$.

Further supporting the NCI trends were QTAIM findings which revealed that the electron densities at the bond critical points (BCPs) were similar in magnitude to the corresponding NCI interaction critical points, ρ_{ICP} (see Supporting Information Figure S3, Table S3).

Along with these weak and moderate attractive interactions was a network of H-bonding interactions between the catalyst and substrates that were both more effective at stabilizing the nucleophile and activating the electrophile in the (*Si*)-enantioselective transition states. Consistent with this finding were the larger NBO donor−acceptor orbital interactions which had overall values of 130−131 kcal/mol for *anti*-(1*R*,2*S*)-$\mathbf{TS1}_{\mathbf{C(h)}}$ and *syn*-(1*R*,2*R*)-$\mathbf{TS1}_{\mathbf{C(h)}}$ as opposed to 96−118 kcal/mol values for *anti*-(1*S*,2*R*)-$\mathbf{TS1}_{\mathbf{C(h)}}$ and *syn*-(1*S*,2*S*)-$\mathbf{TS1}_{\mathbf{C(h)}}$, Scheme 2.

C. Effects of Catalyst and Substrate Complementarity and Cooperativity on Enantioselection. While the above findings provide a basis for rationalizing stereocontrol they, nevertheless, leave uncertain a definitive characterization of the binding model which best describes catalyst/substrate recognition and the underlying type of cooperativity implicated in these reactions. In this regard, the archetypical "lock and key" model pioneered by Fischer offers one possible scenario, though given the flexible nature of the HQuin-BAM framework an "induced fit" model would certainly seem more probable. Indeed, the trends arrived at *vide supra* lend strong support to an interesting dependency on matching the shape and size of the catalyst (host molecule) and substrates (guest molecules) upon binding. Moreover, associated with this shape and size matching was the manifestation of cooperativity effects arising from several attractive noncovalent interactions (e.g., H-bonding, weak London dispersive, and stacking interactions) with changes in catalyst conformation. In terms of the computed (*Si*)- vs (*Re*)-transition structures, the importance of these cooperative effects is quite visible. More to the point, in line with an induced fit model, the large dihedral angle (θ_{NCCN} > 50.0°) between the substrates found in the (*Re*)-transition states forced the two quinolinium rings of catalyst to reside far away from one another generating significant strain in the

DOI: 10.1021/acs.joc.6b00248
J. Org. Chem. 2016, 81, 3286−3295

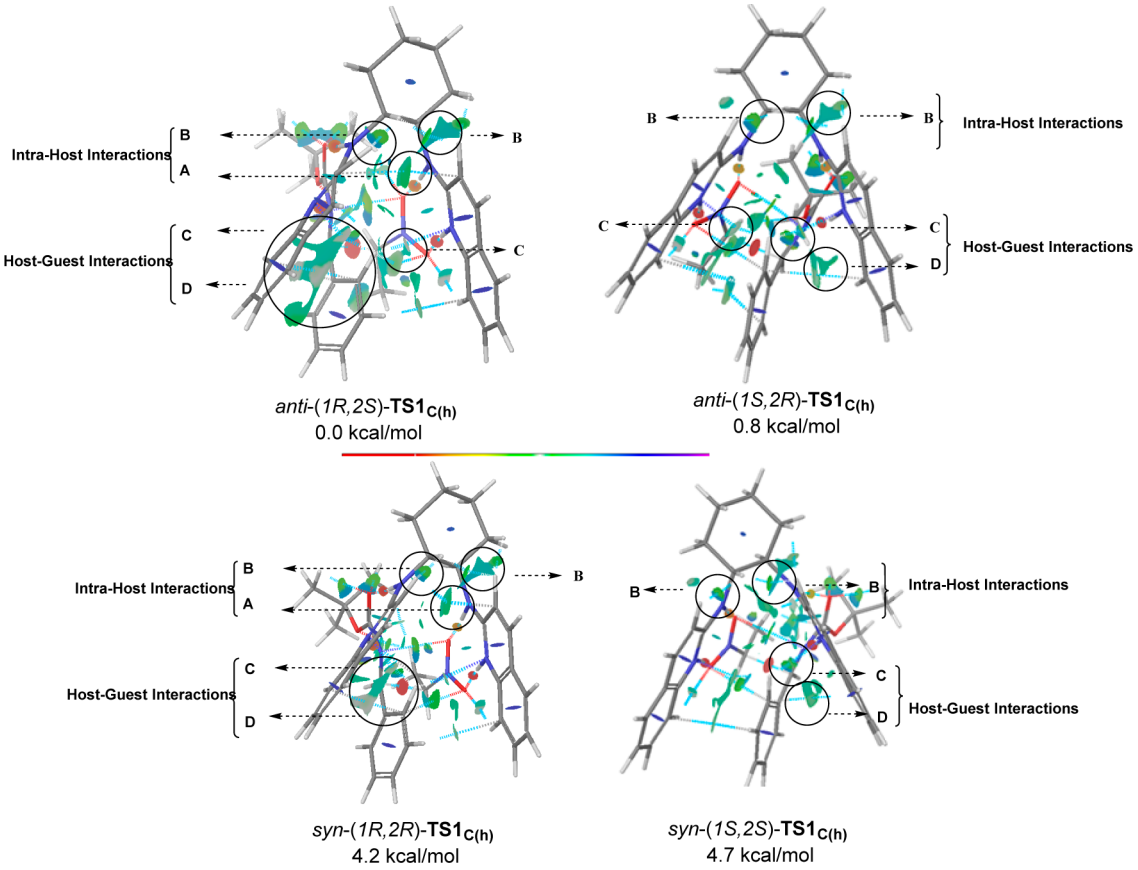

Figure 5. Calculated gradient isosurfaces with s = 0:5 au representing noncovalent interactions. The surfaces are colored on a rainbow scale based on values of sign(λ_2) between −0.04 to 0.04 au.

Scheme 2. Calculated NBO Donor−Acceptor Orbital Interactions Present in the H-Bonding Networks of TS1$_{C(h)}$

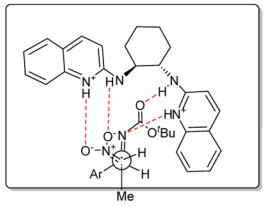

anti-(*1R,2S*)-**TS1**$_{C(h)}$ 0.0 kcal/mol	Bond Distance (Å)	ΔE_{NBO} (kcal/mol)
O...(N)H	1.79	29.5
N...(N$^+$)H	1.83	28.0
O...(N)H	1.81	30.0
O...(N$^+$)H	1.70	43.6
ΔE_{NBO}(total)		**131.1**

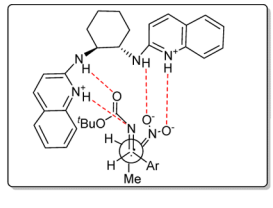

anti-(*1S,2R*)-**TS1**$_{C(h)}$ 0.8 kcal/mol	Bond Distance (Å)	ΔE_{NBO} (kcal/mol)
O...(N)H	1.82	14.4
N...(N$^+$)H	1.76	32.0
O...(N)H	1.85	17.3
O...(N$^+$)H	1.69	33.0
ΔE_{NBO}(total)		**96.7**

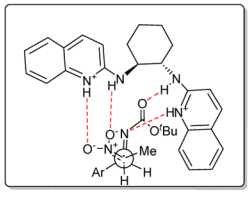

syn-(*1R,2R*)-**TS1**$_{C(h)}$ 4.2 kcal/mol	Bond Distance (Å)	ΔE_{NBO} (kcal/mol)
O...(N)H	1.76	33.0
N...(N$^+$)H	1.88	23.7
O...(N)H	1.84	27.2
O...(N$^+$)H	1.67	46.4
ΔE_{NBO}(total)		**130.3**

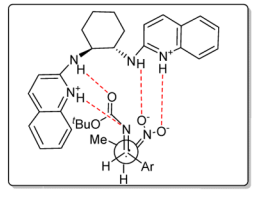

syn-(*1S,2S*)-**TS1**$_{C(h)}$ 4.7 kcal/mol	Bond Distance (Å)	ΔE_{NBO} (kcal/mol)
O...(N)H	1.88	15.8
N...(N$^+$)H	1.77	36.2
O...(N)H	1.79	27.5
O...(N$^+$)H	1.69	39.1
ΔE_{NBO}(total)		**118.6**

DOI: 10.1021/acs.joc.6b00248
J. Org. Chem. 2016, 81, 3286−3295

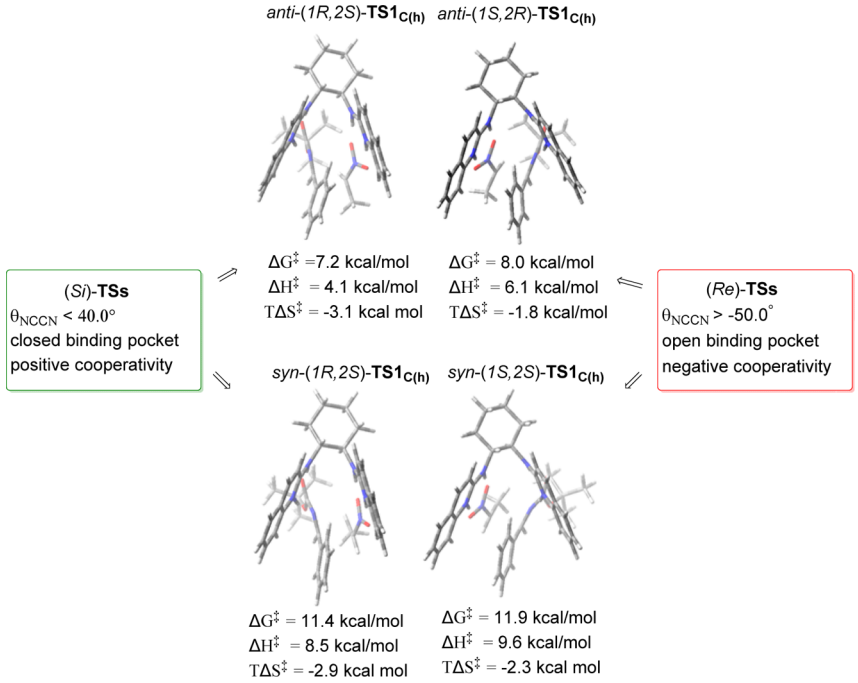

Figure 6. Effects of catalyst and substrate complementarity and cooperativity on activation parameters.

catalyst (*vide supra*). Consequently, to compensate for this buildup of strain incurred by conformational changes in the catalyst, the energetics of substrate binding must become more favorable. However, in this case as a result of the opened state of the catalyst binding pocket, which attenuates the importance of attractive noncovalent interactions, this balancing act of energetics is not satisfied and in turn less effective binding is observed. In stark contrast, the observed proper synclinal alignment (θ_{NCCN} < 40.0°) of the substrates in the favorable (*Si*)-transition states allows for the two quinolinium rings of the catalyst to reside nearer to one another forming a more closed binding pocket (as indicated in part B), resulting in less strain and enhanced attractive noncovalent interactions. Combined these last two aspects lead to more effective binding as reflected in lower activation barriers compared to the (*Re*)-transition states (Figure 6). Accordingly, a careful analysis of the Gibbs free energy ($\Delta G^{\ddagger}$) and enthalpic ($\Delta H^{\ddagger}$) activation parameters of the optimized *anti*-(1*R*,2*S*), *anti*-(1*S*,2*R*), *syn*-(1*R*,2*R*), and *syn*-(1*S*,2*S*)-transition states, **TS1**$_{C(h)}$, proved insightful, as it revealed a more favorable enthalpy ($\Delta H^{\ddagger}$ = 4.1, 6.1, 8.5, and 9.6 kcal mol^{-1}) and free energies of activation ($\Delta G^{\ddagger}$ = 7.2, 8.0, 11.4, and 11.9 kcal mol^{-1}) occurred with a small entropic energy penalty ($T\Delta S^{\ddagger}$ = −3.1, −1.8, −2.9, and −2.3 kcal mol^{-1}), respectively.[30] These findings supported the significance of positive cooperative binding observed in the (*Si*)-transition states which was associated with a benefit in enthalpy and a cost in entropy, whereas the negative cooperative binding in the (*Re*)-transition states was accompanied by a cost in enthalpy and a benefit in entropy.[31]

Enantioselective HQuin-BAM Catalyzed Aza-Henry Reactions of Nitroethane with other *N*-Boc Aldimines. As final action to gauge the universality of the insight arrived at from the stereodetermining transition state structures for addition of nitronate **2** to *N*-Boc aldimine **3a**, the corresponding HQuin-BAM catalyzed additions of monoalkylated nitronate to *p*-Cl- and *p*-NO_2-substituted aldimine electrophiles **3b**−**c** were modeled to provide a related series of first-order saddle points **TS2**$_{C(h)}$−**TS3**$_{C(h)}$ (see Supporting Information for structural details).[32]

Initially, the most encouraging finding from these calculations was that the predicted preferred sense of (1*R*,2*S*)-stereoinduction was consistent with that computed for nitronate addition to **3a** and reported experimentally.[13a] Meanwhile the overall structural features of *anti*-(1*R*,2*S*)-**TS2**$_{C(h)}$ and *anti*-(1*R*,2*S*)-**TS3**$_{C(h)}$ were similar to those of *anti*-(*R*,*S*)-**TS1**$_{C(h)}$ in most respects as seen by the synclinal dihedral angles of 38.8° and 38.0° around the forming C−C bonds of the substrates in the former two transition states and the θ_{NCCN} of 38.8° found in the latter. Allied with these synclinal alignments, notably, were favorable donor−acceptor interactions originating from nitronate oxygen lone pair donation into antibonding orbitals of the C═O and N═C bonds of the *N*-Boc aldimines (see Supporting Information). Mirroring *anti*-(1*R*,2*S*)-**TS1**$_{C(h)}$ as well were closed catalyst binding pockets in *anti*-(1*R*,2*S*)-**TS2**$_{C(h)}$ and *anti*-(1*R*,2*S*)-**TS3**$_{C(h)}$, which reinforced the intramolecular (intrahost) and intermolecular (host−guest) noncovalent attractive interactions. Attesting to this fact were the $C_{(ring\ 1)}$−$C_{(ring\ 2)}$ ≈ 4.40 Å and $C_{(ring\ 3)}$−$C_{(ring\ 4)}$ ≈ 6.30 Å distances, as well as larger ρ_{ICP} values stemming from intramolecular London dispersive $\pi_{Ar}\cdots\pi_{Ar}$ interactions in *anti*-(1*R*,2*S*)-**TS2**$_{C(h)}$ (ρ_{ICP} = −0.0038) and *anti*-(1*R*,2*S*)-**TS3**$_{C(h)}$ (ρ_{ICP} = −0.0041) vs *anti*-(1*R*,2*S*)-**TS1**$_{C(h)}$ (ρ_{ICP} = −0.0037), Figure 7. Present also were intermolecular (host−guest) $\pi_{Ar}\cdots\pi_{Ar}$ or $C-H_{Ar}\cdots\pi_{Ar}$ stacking interactions involving the *N*-Boc aldimine and quinolinium rings of the catalyst. Notably, these interactions were larger in *anti*-(1*R*,2*S*)-**TS2**$_{C(h)}$ and *anti*-(1*R*,2*S*)-**TS3**$_{C(h)}$ relative to *anti*-(1*R*,2*S*)-**TS1**$_{C(h)}$ as judged from the ρ_{ICP} values of −0.0068, −0.0069, and −0.0067 in each transition state, respectively. Also apparent were $N^{+}-H\cdots\pi_{Ar}$ interactions between the catalyst and substrates as assessed from the ρ_{ICP} of −0.0071, −0.0074, and −0.0069. Ultimately, the stronger noncovalent interactions in *anti*-(1*R*,2*S*)-**TS2**$_{C(h)}$ and *anti*-(1*R*,2*S*)-**TS3**$_{C(h)}$ relative to *anti*-(1*R*,2*S*)-**TS1**$_{C(h)}$ had the consequence of reducing the

DOI: 10.1021/acs.joc.6b00248
J. Org. Chem. 2016, 81, 3286−3295

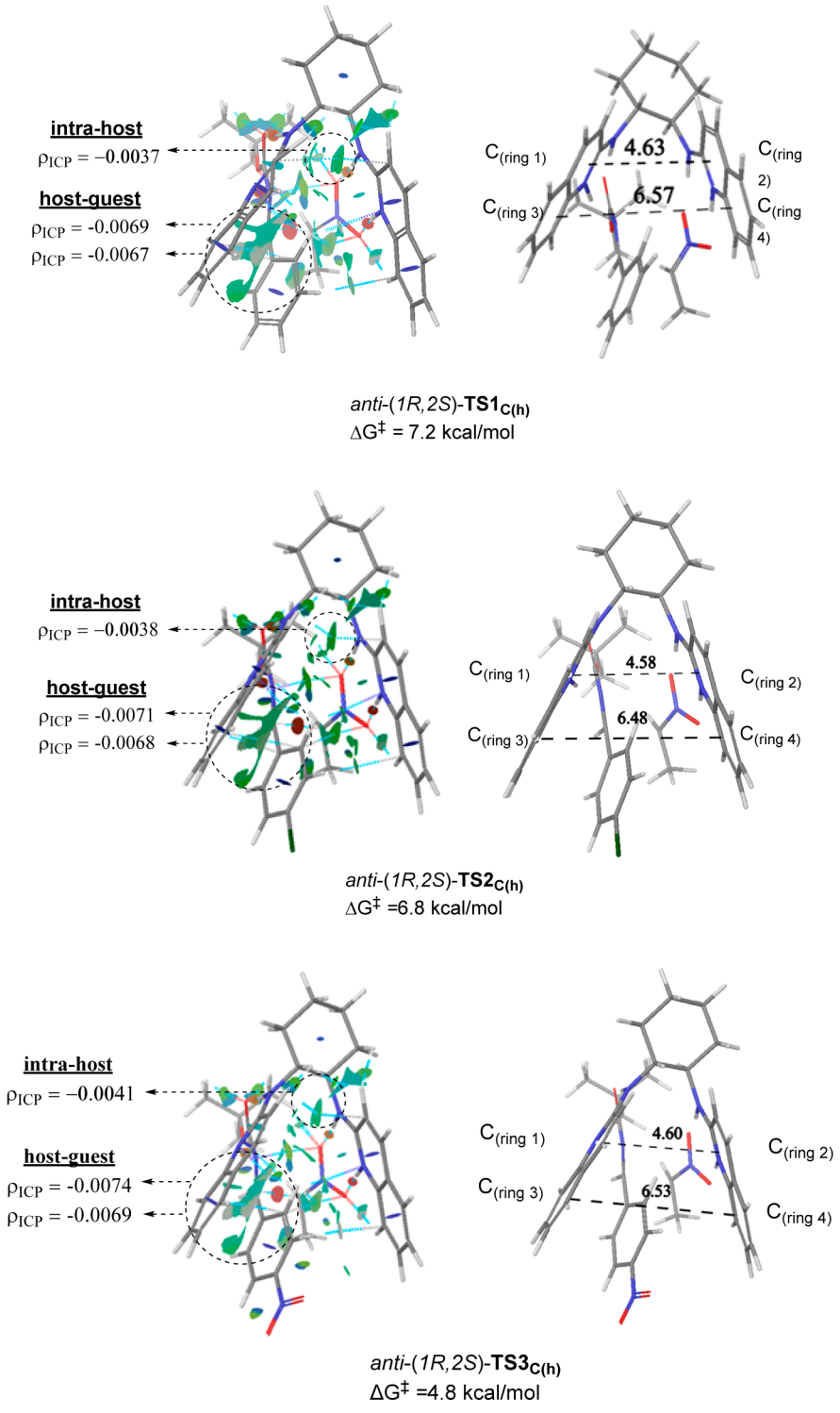

Figure 7. Comparison of C−C bond forming substituted transition states with unsubstituted transition state structures (*anti*-(1*R*,2*S*)-**TS2**$_{C(h)}$ and *anti*-(1*R*,2*S*)-**TS3**$_{C(h)}$ relative to *anti*-(1*R*,2*S*)-**TS1**$_{C(h)}$).

activation barriers for C−C bond formation. Moreover, the associated activation barriers for *anti*-(1*R*,2*S*)-**TS1**$_{C(h)}$−**TS3**$_{C(h)}$ were 7.2, 6.8, and 4.8 kcal/mol, respectively (Figure 7).

Take together it is apparent from these findings that the inclusion of electron-withdrawing *p*-Cl- and *p*-NO_2-substituents on the *N*-Boc aldimine aryl ring had a significant impact upon host−guest recognition, as observed by the enhancement of attractive noncovalent interactions between the quinolinium fragments of the catalyst and substrate aryl rings of **3b**−**c** compared to the unsubstituted phenyl group of **3a**. Importantly, this increase in noncovalent interactions materialized in a lowering of activation barriers.

CONCLUSIONS

In conclusion, the density functional theory (DFT) study reported here provides support for the role of cooperative effects arising from multiple noncovalent interactions as key factors governing stereoinduction in HQuin-BAM (**1**) catalyzed

DOI: 10.1021/acs.joc.6b00248
J. Org. Chem. 2016, 81, 3286−3295

aza-Henry reactions. Associated with these attractive interactions was a size and shape dependency between the catalyst and substrates that when matched resulted in a closed catalyst binding pocket and a substrate alignment that optimally was synclinal. Notably, this complementary relationship led to improved substrate binding which in conjunction with stereoelectronic effects and dispersive forces was the dominant factor for enantioinduction, as reflected in favorable activation parameters. The magnitude of these noncovalent interactions was found to be sensitive to the nature of the *N*-Boc aldimine aryl group, which in turn affected enantioselection. Meanwhile, unfavorable steric interactions formed the basis for diastereoselection. It is anticipated that the in-depth rationale offered here will serve as a guide for designing a novel H-bond organocatalyst utilizing several attractive noncovalent interactions as a key driving force for promoting asymmetric processes.

■ ASSOCIATED CONTENT

Supporting Information

The Supporting Information is available free of charge on the ACS Publications website at DOI: 10.1021/acs.joc.6b00248.

Computed coordinate and thermochemical data for all structures, as well as QTAIM, NBO, and NCI index analysis (PDF)

■ AUTHOR INFORMATION

Corresponding Author

*E-mail: tdudding@brocku.ca.

Notes

The authors declare no competing financial interest.

■ ACKNOWLEDGMENTS

The authors would like to thank Sharcnet for computing resources. Financial support was provided in part by an NSERC Discover Grant (2014-04410). S.M.T. thanks Thrillium Ontario Scholarship for financial support.

■ REFERENCES

(1) (a) Desiraju, G. R.; Steiner, T. *The Weak Hydrogen Bond in Structural Chemistry and Biology*; Oxford University Press: Oxford, 1999. (b) Pimentel, G. C.; McClellan, A. L. *The Hydrogen Bond*; Freeman: San Francisco, 1960. (c) Jeffrey, G. A. *An Introduction to Hydrogen Bonding*; Oxford University: New York, 1997. (d) Silverman, R. B. *The Organic Chemistry of Enzyme Catalyzed Reactions*; Academic: San Diego, CA, 2002.

(2) (a) Schreiner, P. R. *Chem. Soc. Rev.* **2003**, *32*, 289. (b) Taylor, M. S.; Jacobsen, E. N. *Angew. Chem., Int. Ed.* **2006**, *45*, 1520−1543. (c) Doyle, A. G.; Jacobsen, E. N. *Chem. Rev.* **2007**, *107*, 5713−5743. (d) Liu, X.; Lin, L.; Feng, X. *Chem. Commun.* **2009**, 6145−6158. (e) Cheong, P. H.-Y.; Legault, C. Y.; Um, J. M.; Celebi-Olcum, N.; Houk, K. N. *Chem. Rev.* **2011**, *111*, 5042−5137.

(3) (a) Schuster, T.; Kurz, M.; Göbel, M. W. *J. Org. Chem.* **2000**, *65*, 1697. (b) Schuster, T.; Kurz, M.; Göbel, M. W. *J. Org. Chem.* **2000**, *65*, 1697. (c) Sohtome, Y.; Hashimoto, Y.; Nagasawa, K. *Adv. Synth. Catal.* **2005**, *347*, 1643. (d) Terada, M.; Nakano, M.; Ube, H. *J. Am. Chem. Soc.* **2006**, *128*, 16044. (e) Mirabdolbaghi, R.; Hassan, M.; Dudding, T. *Tetrahedron: Asymmetry* **2015**, *26*, 560.

(4) (a) Hafez, A. M.; Dudding, T.; Wagerle, T. R.; Shah, M. H.; Taggi, A. E.; Lectka, T. *J. Org. Chem.* **2003**, *68*, 5819. (b) Sengupta, A.; Sunoj, R. B. *J. Org. Chem.* **2012**, *77*, 10525. (c) Wei, Y.; He, W.; Liu, Y.; Liu, P.; Zhang, S. *Org. Lett.* **2012**, *14*, 704. (d) Hintermann, L.; Ackerstaff, J.; Boeck, F. *Chem. - Eur. J.* **2013**, *19*, 2311. (e) Lam, Y.-H.; Houk, K. N. *J. Am. Chem. Soc.* **2014**, *136*, 9556.

(5) (a) Iyer, M. S.; Gigstad, K. M.; Namdev, N. D.; Lipton, M. *J. Am. Chem. Soc.* **1996**, *118*, 4910. (b) Shvo, Y.; Becker, G. M.; Elgavi, A. *Tetrahedron: Asymmetry* **1996**, *7*, 911. (c) Romney, D. K.; Miller, S. J. *Org. Lett.* **2012**, *14*, 1138. (d) Blank, J. T.; Guerin, D. J.; Miller, S. J. *Org. Lett.* **2000**, *2*, 1247.

(6) (a) Yalalov, D. A.; Tsogoeva, S. B.; Schmatz, S. *Adv. Synth. Catal.* **2006**, *348*, 826. (b) Hamza, A.; Schubert, G.; Soos, T.; Papai, I. *J. Am. Chem. Soc.* **2006**, *128*, 13151. (c) Kitagaki, S.; Ueda, T.; Mukai, C. *Chem. Commun.* **2013**, *49*, 4030. (d) Breugst, M.; Houk, K. N. *J. Org. Chem.* **2014**, *79*, 6302.

(7) (a) Weinhold, F.; Klein, R. A. *Mol. Phys.* **2012**, *110*, 565. (b) Weinhold, F.; Klein, R. A. *Chem. Educ. Res. Pract.* **2014**, *15*, 276. (c) O'Meara, M. J.; Leaver-Fay, A.; Tyka, M. D.; Stein, A.; Houlihan, K.; DiMaio, F.; Bradley, P.; Kortemme, T.; Baker, D.; Snoeyink, J.; Kuhlman, B. *J. Chem. Theory Comput.* **2015**, *11*, 609.

(8) (a) Lamoureux, J. S.; Maynes, J. T.; Glover, J. N. M. *J. Mol. Biol.* **2004**, *335*, 399. (b) Riley, K. E.; Pitoňák, M.; Jurečka, P.; Hobza, P. *Chem. Rev.* **2010**, *110*, 5023. (c) Takahashi, O.; Kohno, Y.; Nishio, M. *Chem. Rev.* **2010**, *110*, 6049. (d) Knowles, R. R.; Jacobsen, E. N. *Proc. Natl. Acad. Sci. U. S. A.* **2010**, *107*, 20678.

(9) (a) Williams, D. H.; Calderone, C. T.; O'Brien, D. P.; Zerella, R. *Chem. Commun.* **2002**, 1266. (b) Williams, D. H.; Stephens, E.; Zhou, M. *Chem. Commun.* **2003**, 1973. (c) Hunter, C. A.; Anderson, H. L. *Angew. Chem., Int. Ed.* **2009**, *48*, 7488. (d) Alkorta, I.; Blanco, F.; Deyà, P. M.; Elguero, J.; Estarellas, C.; Frontera, A.; Quinonero, D. *Theor. Chem. Acc.* **2010**, *126*, 1.

(10) (a) Fierman, M. B.; O'Leary, D. J.; Steinmetz, W. E.; Miller, S. J. *J. Am. Chem. Soc.* **2004**, *126*, 6967. (b) Zuend, S. J.; Jacobsen, E. N. *J. Am. Chem. Soc.* **2007**, *129*, 15872. (c) Bella, M.; Schietroma, D. M. S.; Cusella, P. P.; Gasperi, T.; Visca, V. *Chem. Commun.* **2009**, 597. (d) Xu, H.; Zuend, S. J.; Woll, M. G.; Tao, Y.; Jacobsen, E. N. *Science* **2010**, *327*, 986.

(11) (a) Williams, D. H.; Davies, N. L.; Zerella, R.; Bardsley, B. *J. Am. Chem. Soc.* **2004**, *126*, 2042. (b) Alkorta, I.; Blanco, F.; Elguero, J. *J. Chem. Theory Comput.* **2009**, *5*, 1186. (c) Carrillo, R.; Feher-Voelger, A.; Martín, T. *Angew. Chem., Int. Ed.* **2011**, *50*, 10616. (d) Carrillo, R.; Morales, E. Q.; Martín, V.; Martín, T. *Chem. - Eur. J.* **2013**, *19*, 7042.

(12) (a) Schuster, T.; Bauch, M.; Durner, G.; Göbel, M. W. *Org. Lett.* **2000**, *2*, 179. (b) Tsogoeva, S. B.; Durner, G.; Bolte, M.; Göbel, M. W. *Eur. J. Org. Chem.* **2003**, *2003*, 1661. (c) Akalay, D.; Durner, G.; Bats, J. W.; Bolte, M.; Göbel, M. W. *J. Org. Chem.* **2007**, *72*, 5618.

(13) (a) Nugent, B. M.; Yoder, R. A.; Johnston, J. N. *J. Am. Chem. Soc.* **2004**, *126*, 3418. (b) Hess, A. S.; Yoder, R. A.; Johnston, J. N. *Synlett* **2006**, *1*, 147. (c) Dobish, M. C.; Johnston, J. N. *Org. Lett.* **2010**, *12*, 5744. (d) Shen, B.; Makley, D. M.; Johnston, J. N. *Nature* **2010**, *465*, 1027. (e) Davis, T. A.; Johnston, J. N. *Chem. Sci.* **2011**, *2*, 1076. (f) Davis, T. A.; Danneman, M. W.; Johnston, J. N. *Chem. Commun.* **2012**, *48*, 5578. (g) Davis, T. A.; Vilgelm, A. E.; Richmond, A.; Johnston, J. N. *J. Org. Chem.* **2013**, *78*, 10605. (h) Vara, B. A.; Mayasundari, A.; Tellis, J. C.; Danneman, M. W.; Arredondo, V.; Davis, T. A.; Min, J.; Finch, K.; Guy, R. K.; Johnston, J. N. *J. Org. Chem.* **2014**, *79*, 6913.

(14) Belding, L.; Taimoory, S. M.; Dudding, T. *ACS Catal.* **2015**, *5*, 343.

(15) Gilli, P.; Pretto, L.; Bertolasi, V.; Gilli, G. *Acc. Chem. Res.* **2009**, *42*, 33.

(16) Frisch, M. J.; Trucks, G. W.; Schlegel, H. B.; Scuseria, G. E.; Robb, M. A.; Cheeseman, J. R.; Scalmani, G.; Barone, V.; Mennucci, B.; Petersson, G. A.; Nakatsuji, H.; Caricato, M.; Li, X.; Hratchian, H. P.; Izmaylov, A. F.; Bloino, J.; Zhang, G.; Sonnenberg, J. L.; Hada, M.; Ehara, M.; Toyota, K.; Fukuda, R.; Hasegawa, J.; Ishida, M.; Nakajima, T.; Honda, Y.; Kitao, O.; Nakai, H.; Vreven, T.; Montgomery, J. A.; Peralta, Jr., J. E.; Ogliaro, F.; Bearpark, M.; Heyd, J. J.; Brothers, E.; Kudin, K. N.; Staroverov, V. N.; Kobayashi, R.; Normand, J.; Raghavachari, K.; Rendell, A.; Burant, J. C.; Iyengar, S. S.; Tomasi, J.; Cossi, M.; Rega, N.; Millam, J. M.; Klene, M.; Knox, J.e.; Cross, J. B.; Bakken, V.; Adamo, C.; Jaramillo, J.; Gomperts, R.; Stratmann, R. E.; Yazyev, O.; Austin, A. J.; Cammi, A. R.; Pomelli, C.; Ochterski, J. W.; Martin, R. L.; Morokuma, K.; Zakrzewski, V. G.; Voth, G. A.;

DOI: 10.1021/acs.joc.6b00248
J. Org. Chem. 2016, 81, 3286−3295

Salvador, P.; Dannenberg, J. J.; Dapprich, S.; Daniels, A. D.; Farkas, Ö.; Foresman, J. B.; Ortiz, J. V.; Cioslowski, J.; Fox, D. J. *Gaussian 09*, Revision D.02; Gaussian, Inc., Wallingford, CT, 2009.
(17) (a) Grimme, S. *Wiley Interdiscip. Rev. Comput. Mol. Sci.* **2011**, *1*, 211. (b) Grimme, S.; Antony, J.; Ehrlich, S.; Krieg, H. *J. Chem. Phys.* **2010**, *132*, 154104. (c) Grimme, S. *J. Comput. Chem.* **2004**, *25*, 1463. (d) Grimme, S. *J. Comput. Chem.* **2006**, *27*, 1787.
(18) Chai, J.-D.; Head-Gordon, M. *Phys. Chem. Chem. Phys.* **2008**, *10*, 6615.
(19) Tomasi, J.; Mennucci, B.; Cances, E. *J. Mol. Struct.: THEOCHEM* **1999**, *464*, 211.
(20) Zhao, Y.; Truhlar, D. G. *Phys. Chem. Chem. Phys.* **2008**, *10*, 2813.
(21) (a) Reed, A. E.; Weinstock, R. B.; Weinhold, F. *J. Chem. Phys.* **1985**, *83*, 735. (b) Glendening, E. D.; Reed, A. E.; Carpenter, J. E.; Weinhold, F. *NBO*, version 3.1; University of Wisconsin: Madison, WI, 1990.
(22) Bader, R. F. W. *Atoms in Molecules, A Quantum Theory*; Oxford University Press: Oxford, 1990.
(23) *Schrödinger Materials Science Suite 2014-2*; Schrödinger, LLC, New York, NY, 2014.
(24) (a) Usharani, D.; Lacy, D. C.; Borovik, A. S.; Shaik, S. *J. Am. Chem. Soc.* **2013**, *135*, 17090. (b) Green, A. G.; Liu, P.; Merlic, C. A.; Houk, K. N. *J. Am. Chem. Soc.* **2014**, *136*, 4575.
(25) Despite repeated attempts two transition states conforming to energetically unfavorable *anti*-(*1S,2R*) and *syn*-(*1S,2S*)-transition state structures could not be located, due to the respective starting geometries converging on other modes of addition or difficulties with optimizations.
(26) (a) Johnston, R. C.; Cheong, P. H-Y. *Org. Biomol. Chem.* **2013**, *11*, 5057. (b) Paton, R. S. *Org. Biomol. Chem.* **2014**, *12*, 1717.
(27) (a) Johnson, E. R.; Mackie, I. D.; DiLabio, G. A. *J. Phys. Org. Chem.* **2009**, *22*, 1127. (b) Kruse, H.; Goerigk, L.; Grimme, S. *J. Org. Chem.* **2012**, *77*, 10824. (c) Hobza, P. *Acc. Chem. Res.* **2012**, *45*, 663. (d) Johnston, R. C.; Cheong, P. H.-Y. *Org. Biomol. Chem.* **2013**, *11*, 5057. (e) Armstrong, A.; Boto, R.; Dingwall, P.; Contreras-García, J.; Harvey, M. J.; Mason, N. J.; Rzepa, H. S. *Chem. Sci.* **2014**, *5*, 2057. (f) Soniat, M.; Rogers, D. M.; Rempe, S. B. *J. Chem. Theory Comput.* **2015**, *11*, 2958.
(28) Wang, Y.; Wang, J.; Yao, L. *J. Phys. Chem. A* **2015**, *119*, 3471.
(29) (a) Johnson, E. R.; Keinan, S.; Mori-Sánchez, P.; Contreras-García, J.; Cohen, A. J.; Yang, W. *J. Am. Chem. Soc.* **2010**, *132*, 6498. (b) Contreras-García, J.; Johnson, E. R.; Keinan, S.; Chaudret, R.; Piquemal, J.-P.; Beratan, D. N.; Yang, W. *J. Chem. Theory Comput.* **2011**, *7*, 625.
(30) The activation parameters for these stereodetermining transition states were evaluated with respect to the ternary complex of catalyst−aldimine−nitroethane.
(31) Williams, D. H.; Stephens, E.; O'Brien, D. P.; Zhou, M. *Angew. Chem., Int. Ed.* **2004**, *43*, 6596.
(32) The structures and relative energies of the stereodetermining transition states, $\mathbf{TS4}_{C(h)}$−$\mathbf{TS5}_{C(h)}$, for monoalkylated nitronate addition to *p*-OCF_3- and *m*-NO_2-substituted aldimines can also be found in the Supporting Information. The preferred sense of (1*R*,2*S*)-stereoinduction, the overall energetic trends, and structural features of these stereodetermining transition states were consistent with those of $\mathbf{TS1}_{C(h)}$−$\mathbf{TS3}_{C(h)}$ (see Supporting Information). Although the focus of this work was on determining the origin of selectivity in the aza-Henry reaction of nitroethane with different aldimines for comparison, we have also modeled the transition states for the reaction of nitromethane with *p*-NO_2-substituted aldimine, $\mathbf{TS6}_{C(h)}$ (see Supporting Information, Section 5).

DOI: 10.1021/acs.joc.6b00248
J. Org. Chem. 2016, 81, 3286−3295